Modeling of Electron and Lattice Temperature Distribution Through Lifetime of Plasma Plume

Chief of Engineers: Ali Hamza Alwan Al-taee
Gas Filling Company
Ministry of Oil
Email: alihaltaee@yahoo.com

ABSTRACT

When employing shorter (sub picosecond) laser pulses, in ablation kinetics the features appear which can no longer be described in the context of the conventional thermal model. Meanwhile, the ablation of materials with the aid of ultra-short (sub picosecond) laser pulses is applied for micromechanical processing.

Physical mechanisms and theoretical models of laser ablation are discussed. Typical associated phenomena are qualitatively regarded and methods for studying them quantitatively are considered. Calculated results relevant to ablation kinetics for a number of substances are presented and compared with experimental data. Ultra short laser ablation with two-temperature model was quantitatively investigated. A two-temperature model for the description of transition phenomena in a non-equilibrium electron gas and a lattice under picosecond laser irradiation is proposed. Some characteristics are hard to measure directly at all. That is why the analysis of physical mechanisms involved in the ablation process by ultra-short laser pulses has to be performed on the basis of a theoretical consideration of `indirect' experimental data.

For Copper and Nickel metal targets, the two-temperature model calculations explain that the temperature of the electron subsystem increased suddenly and approached a peak value at the end of laser pulse. In addition, the temperature profile of lattice temperature subsystem evolution slowly, and still increasing after the end of laser pulse. A good agreement prevails when a comparison between the present results and published results.

Key words: pulsed laser, heat ablation by laser, two-temperature model, plasma plume.

نمذجة توزيع درجة حرارة الالكترونات و الشبكة خلال فترة تكون غيمة البلازما

رئيس مهندسين: **علي حمزة علوان الطائي**
شركة تعبئة الغاز
وزارة النفط

الخلاصة

عند استخدام نبضات الليزر ألقصيرة (اقل من 10^{-12} Sec.)، في حركية التذرية تظهر خصائص لا يمكن وصفها في سياق النماذج الحرارية التقليدية. لذا فان تشغيل المعادن الميكانيكي (بمقاييس مايكروية) يتم انجازه بتذرية المواد بدعم نبضات الليزر فائقة القصر (اقل من بيكو ثانية).

في البحث الحالي تم مناقشة الآليات الفيزيائية والنماذج النظرية للتذرية بواسطة المصادر الليزرية المنبضة. الظواهر النموذجية المرافقة تعتبر نوعية و تم بحثها بطرق كمية. لعدد من المواد, النتائج ذات الصلة بحركية التذرية تم عرضها ومقارنتها مع البيانات التجريبية المنشورة سابقا واظهرت توافق جيد. التذرية بواسطة المصادر الليزرية المنبضة فائقة القصر تمت دراستها باستخدام نموذج ثنائي درجة الحرارة وكان التحليل كمي. لبيان الظواهر غير المتوازنة و الانتقالية لخليط " غاز الالكترونات-الايون" بسبب الإشعاع الساقط من مصادر ليزرية منبضة فائقة القصر قد تم اقتراح استخدام النموذج ثنائي درجة الحرارة. بعض الخواص يصعب قياسها بشكل مباشر. لذا فان دراسة آلية عمل التذرية بواسطة المصادر الليزرية المنبضة قد تم انجازها بمراعاة الاعتبارات النظرية غير المباشرة التي تم الحصول عليها من تجارب عملية سابقة.

الحسابات النظرية باستخدام نموذج ثنائي درجة الحرارة بينت ان درجة حرارة الالكترونات تزداد بشكل سريع و مفرط وتصل لاقصى قيمة عند نهاية نبضة الليزر عند استخدام النحاس او النيكل كمعدن هدف. تزداد درجة حرارة الشبكة في نهاية زمن نبضة الليزر, وتستمر بالتنامي بعد انتهاء النبضة. قيمة درجة حرارة الشبكة دائما اقل من درجة حرارة الالكترونات. ضعف الترابط بين الالكترونات و الشبكة يؤدي الى انخفاض معدل التذرية خلال زمن نبضة الليزر.

الكلمات الرئيسية: ليزر منبض, تذرية بالليزر, نموذج ثنائي درجة الحرارة, غيمة البلازما.

1. INTRODUCTION

Ablation occurred when solid surface exposure to an intense laser irradiation. As a result atoms or clusters may emit from the target surface. For the ultra-short laser pulse duration, there is a variation in the temperature between electrons and lattice sub-systems. Two temperature model one of the approaches can be applied to investigate the temperature profiles throughout the laser target.

Schäfer, et al., 2002, investigated picosecond laser ablation of metals by using a hybrid simulation scheme. Laser energy input into the electron system and heat conduction within it are modeled using a finite-difference scheme for solving the heat conduction equation. Energy transfer between the electronic and atomic subsystems due to electron-phonon coupling is taken into account. **Zhigilei, et al., 2002,**discussed two computational schemes developed for simulation of laser coupling to organic materials and metals and present a multi-scale model for laser ablation and cluster deposition of nano-structured materials. For metals, the two temperature model coupled to the atomistic (molecular dynamics) MD model provides an adequate description of the laser energy absorption into the electronic system and fast electron heat conduction. **Korte, et al., 2000,** investigated the production sub-diffraction limited structures in thin metal films and bulk dielectric materials using femtosecond laser pulses. The physics of ultrashort pulse laser ablation of solids is outlined. They reported the results on the fabrication of sub-micrometer structures in 100-200 nm chrome-coated surfaces by direct ablation.

Anisimov, et al., 1996, performed the ablation of Cu and Al targets with 170 fs laser pulses in the intensity range of 1012-1014 W/cm^2. They compare the measured removal depth with 1D hydrodynamic simulations. The electron-ion temperature decoupling is taken into account using the standard two-temperature model.

Bulgakova, et al., 2007, presented a number of numerical models, which have been developed to describe the processes taking place at different time and length scales in different classes of materials under the irradiation by ultra-short laser pulses. The two-temperature model is used to follow heating dynamics of irradiated matter and to analyze its phase transformations on the basis of thermodynamic concepts.

Chimmalgi, et al., 2005, simulated a numerical calculations insight into the spatial distribution of the enhanced field intensity underneath the tip and associated physical phenomena. Calculate the temperature distribution in the microprobe tip and possible tip expansion. **Hermann, et al., 2005,** investigated micromachining of CuInSe2 (CIS)-based photovoltaic devices with short and ultra-short laser pulses. Therefore, ablation thresholds and ablation rates of ZnO, Mo and CuInSe2 thin films have been measured for irradiation with nanosecond laser pulses of ultraviolet and visible light and sub-picosecond laser pulses of a Ti:sapphire laser. The experimental results were compared to the theoretical evaluation of the samples heat regime.

Leitz, et al., 2011, presented contribution a comparative study of the ablation of metal with micro-, nano-, pico and femtosecond laser pulses. In ultra-short pulse

laser ablation extreme pressures, densities and temperatures build up and accelerate the ionized material to enormous velocities. Due to the short interaction time the material cannot evaporate continuously but is transferred into a state of overheated liquid. This merges into a high pressure mixture of liquid droplets and vapor expanding rapidly.

Ultra-short laser pulses provide unique possibilities for high-precision material processing. Due to rapid energy delivery, localized heat-affected zone, and minimal residual damage. As a result, numbers of numerical models are presented which have been developed to describe the processes taking place at different time and length scales in different classes of materials under the irradiation by ultra-short laser pulses.

Pulsed laser ablation is the process of material removal, after the target irradiated by intensive laser pulses. The short pulse duration confines heat diffusion, which leads to high-quality machining. Sharp-edged, clean and highly reproducible machining results have obtained using a femtosecond laser.

When the laser irradiation strike the metal targets. There are three energy transfer stages during femtosecond laser ablation, **Harrach, 1977.** These stages are:

1. The free electrons absorb the energy from the laser. This stage characterized by a lack of thermal equilibrium among the electrons.
2. The electrons reach thermal equilibrium and the density of states can now represented by the Fermi distribution. However, electrons and the lattice are still at two different temperatures.
3. Electron and lattice reach thermal equilibrium and thermal diffusion carries the energy into the bulk.

This mechanism can be represented geometrically by a large block of material subjected to short pulse of laser beam radiation. The power of the laser beam is incidents on the surface of the material, over a circular area ($r_{ab}^2\pi$). Then the material absorbs the energy. The absorbed energy will interacts with the material as above. Where, the energy diffuses through the material in all dimensions. Through the material, the temperature profile rises from the room temperature to a very high value. A phase transition process will occurred.

The effects of the absorbed laser energy by material were represented by a source term in the energy equation analysis, **Schäfer, et al., 2002. Fig. 1.b,** showed the cylindrical coordinates system for semi-infinite medium.

In the present study the two-temperature model with nonlinear change in physical properties is modeled. A comparison study is carried out. This study explain the effect of every physical quantity "property" in the performance of temperature evolution for every sub-system "free electron and lattice".

2. MATHEMATICAL MODEL

Laser ablation cannot be described within a single computational model **Zhigilei, et al., 2002.** The two-temperature models used to predict the non-equilibrium. **Anisimov, et al., 1996.** and, **Qiu,** and **Tien, 1993.** First described the temperature distribution between electrons and, lattice during femtosecond laser irradiation of metals. The two-temperature model looks at the heating mechanism as; initially due to inverse- Bremsstrahlung the laser energy is absorbed by free electrons. The absorption followed by a fast energy relaxation within the electronic subsystem, thermal diffusion and an energy transfer to the lattice due to electron-phonon coupling. Under the following assumptions:

1. When the laser beam incident vertically on the material surface i.e. axi-symmetric the material will be isotropic $\frac{\partial}{\partial\theta} = 0$, **Al-moosawy, 2002.** As indicated in **Fig. 1.a.**
2. Neglecting the material thermal expansion completely and declaring that one needs a definite amount of energy to initiate ablation, **Alan, and David, 1973.**
3. The present investigation achieved per pulse.
4. The time scale is less than the time for energy transfer from the electrons to the lattice, **Schäfer, et al., 2002.** Therefore there is a temperature shift between electron and lattice sub-systems.
5. For calculation, the laser beam is considered as uniform in space with temporal Gaussian distribution, **Cheng, and Xu, 2005.**
6. Near the critical point, the temperature dependent properties nor available always, therefore some of the material properties is considered as not temperature dependent. Moreover, the uncertainties in the properties will not affect this study since the focus is on the mechanism of laser ablation.
7. The laser beam is incident vertically on the surface of the target material. In other words, the angle of incident equals zero.

Through the cylindrical coordinates system; the following three-dimensional equations are described spatial and temporal evolution of the electron and lattice temperature in a material. They treat electrons and lattice as two separate sub-systems with different temperatures.

1. For electron sub-system:

$$C_e\left(\frac{\partial T_e}{\partial t}\right) = K_e\left(\frac{\partial^2 T_e}{\partial r^2} + \frac{1}{r}\frac{\partial T_e}{\partial r} + \frac{1}{r^2}\frac{\partial^2 T_e}{\partial \theta^2} + \frac{\partial^2 T_e}{\partial z^2}\right) - \gamma(T_e - T_l) + S_{ab} \quad (1.a)$$

2. For lattice sub-system:

$$C_l\left(\frac{\partial T_l}{\partial t}\right) = K_l\left(\frac{\partial^2 T_l}{\partial r^2} + \frac{1}{r}\frac{\partial T_l}{\partial r} + \frac{1}{r^2}\frac{\partial^2 T_l}{\partial \theta^2} + \frac{\partial^2 T_l}{\partial z^2}\right) + \gamma(T_e - T_l) \quad (1.b)$$

The last term into Eq. (1.a) represents the laser energy absorbed by the material target. The second term in the right hand side (R.H.S) of Eq. (1) represents the rate at which energy exchanges between the two subsystems. The above governing equations are right only with ultrashort laser pulses. Where, in the case of material processing with long laser pulses the electronic and atomic subsystems are in equilibrium i.e. $T_l = T_e$.

2. 1. Further Calculations

1. Fermi temperature is function of material i.e. different for each material. It is calculated as: $T_F = \frac{E_F}{k_B}$ (2)

where the Fermi energy equals $\left[E_F = \frac{1}{2}m v_F^2\right]$ see **Korte, et al., 2002.**

2. The thermal conductivity of the electron and lattice is temperature dependent. **Colombier, et al., 2006. Schäfer, et al., 2002.** and, **Anisimov, et al., 1997.** the electron thermal conductivity commonly expressed as:

$$K_e = \alpha\frac{(\theta_e^2+0.16)^{4/5}(\theta_e^2+0.44)}{(\theta_e^2+0.092)^{1/2}(\theta_e^2+\beta\theta_i)}\theta_e \quad (3)$$

where, θ_e and, θ_l are electron and ion temperature normalized to Fermi temperature ($\theta e=T_e/T_F$, $\theta_l=T_l/T_F$). α and, β are material dependent parameters. When (k_BT_e) remains smaller than the Fermi energy, another equation used to evaluate electronic thermal conductivity **Ashcroft, and Mermin, 1976.** as:

$$K_e = \frac{1}{3} C_e v_F^2 \tau \quad (4)$$

Moreover, the lattice thermal conductivity is dependent on electron and, lattice temperature as follows:

$$K_l = 0.01 \times K_e \quad (5)$$

3. The electronic heat capacity is much less than the lattice heat capacity. Therefore, the electrons can heat to very high transient temperatures. Many equations used to calculate the electronic heat capacity. **Mannion, et al., 2002,** considered it as a function of electron number density: $\left[C_e \approx \frac{3}{2} n_e k_B\right]$ **.Colombier, et al., 2006.** ,and **Korte, et al., 2000** used another equation considers it as a function of electronic temperature and, number density: $\left[C_e \approx \frac{\pi^2}{2}\left(\frac{k_B T_e}{E_F}\right) n_e k_B\right]$ The condition to use this relation is as the condition for use Eq. (5). In the present study, take the electronic heat capacity as a material property.

4. At high fluences and short pulse width, rapid solid-vapor phase change controlled by nucleation dynamics rather than by heat transfer at the phase change interface **Xianfan, 2004.** At the solid-vapor interface, i.e. "superheating/under cooling " , the interface velocity (V_{sv}) can represent as:

$$V_{sv} = \frac{(1-R)\times(J_f/t_P)}{[\rho L_{sv}+\rho C_l(T_b-T_o)]} \quad (6)$$

5. The ablated crater diameter is related to the peak fluence, **Mannion et al., 2001,** as:

$$D_{ab}^2 = 2 \times r_b^2 \times \ln\left(\frac{\emptyset_o}{\emptyset_{th}}\right) \quad (7)$$

where, $\emptyset_o = \frac{2\times J_f}{\pi \times r_b^2}$ and $r_{ab} = \frac{D_{ab}}{2}$

6. The laser-heating source S: This term in Eq. (1.a) represents the laser energy deposition into the electron subsystem, "heat generation term in the governing equation". Several equations suggested evaluating this effect **Zhigilei, et al., 2002.** , **Alan, and David, 1973.** , **Cheng, and Xu, 2005.** , **Xianfan, 2004.** , and **Mannion et al., 2001.** In the present study, one of them selected. This selected equation has the largest number of the parameters affects the incident laser beam. The standard form for the laser pulse with a Gaussian temporal and, spatial distribution , **Alan, and David, 1973.** , **Cheng, and Xu, 2005.** and **Xianfan, 2004.** In the present work the source term equation is:

$$S_{(t,r,z)} = \frac{1}{\sqrt{\pi}} \frac{(1-R)J_f}{t_P \times \delta} \times Exp\left\{-\left[\left(\frac{t-t_o}{t_p}\right)^2 + \left(\frac{\sqrt{r^2+z^2}}{\delta}\right)\right]\right\} \quad (8)$$

As indicated before, **Alan, and David, 1973,** showed that when the cylinder is solid rather than hollow. The third term in the R.H.S of Eq. (1) becomes:

$$\lim_{r\to 0}\left(\frac{1}{r^2}\right)\left(\frac{\partial^2 T}{\partial \phi^2}\right)=\lim_{r\to 0}\left(\frac{\partial}{\partial r}\right)\left(\frac{\partial^2 T}{\partial \phi^2}\right)/2r=\lim_{r\to 0}\left(\frac{\partial^2}{\partial r^2}\right)\left(\frac{\partial^2 T}{\partial \phi^2}\right)/2=0 \qquad (9)$$

Therefore, Eq. (1) can be written as:

$$C_e\left(\frac{\partial T_e}{\partial t}\right)=K_e\left(\frac{\partial^2 T_e}{\partial r^2}+\frac{1}{r}\frac{\partial T_e}{\partial r}+\frac{\partial^2 T_e}{\partial z^2}\right)-\gamma(T_e-T_l)+S_{ab} \qquad (10.a)$$

$$C_l\left(\frac{\partial T_l}{\partial t}\right)=K_l\left(\frac{\partial^2 T_l}{\partial r^2}+\frac{1}{r}\frac{\partial T_l}{\partial r}+\frac{\partial^2 T_l}{\partial z^2}\right)+\gamma(T_e-T_l) \qquad (10.b)$$

Where z is measured along the axis of ejection of the plasma and r radial outwards from the axis. A special consideration must be given to the central node at $r=0$. At $r=0$ the first term in the R.H.S of Eq. (10), $\left(\frac{1}{r}\right)\left(\frac{\partial T}{\partial r}\right)$ is indeterminate. This term can be evaluated by suing L'Hopital's rule.

$$\lim_{r\to 0}\left(\frac{1}{r}\right)\left(\frac{\partial T}{\partial r}\right)=\lim_{r\to 0}\left\{\left(\frac{\partial}{\partial r}\right)\left(\frac{\partial T}{\partial r}\right)/\left(\frac{\partial}{\partial r}\right)(r)\right\}=\left(\frac{\partial^2 T}{\partial r^2}\right) \qquad (11)$$

Thus the governing Eq. (10) can be re-formulated as:

$$C_e\left(\frac{\partial T_e}{\partial t}\right)=K_e\left(\frac{\partial^2 T_e}{\partial r^2}+\frac{\partial^2 T_e}{\partial r^2}+\frac{\partial^2 T_e}{\partial z^2}\right)-\gamma(T_e-T_l)+S_{ab} \qquad (12.a)$$

$$C_l\left(\frac{\partial T_l}{\partial t}\right)=K_l\left(\frac{\partial^2 T_l}{\partial r^2}+\frac{\partial^2 T_l}{\partial r^2}+\frac{\partial^2 T_l}{\partial z^2}\right)+\gamma(T_e-T_l) \qquad (12.b)$$

2. 2. Initial and Boundary conditions

Applying initial and boundary conditions to solves Eq. (12). The electron and lattice initial temperature of the material target equal the ambient temperature. Yet there is no laser beam incident on the material surface **Schäfer, et al., 2002.**

At $t=0$, $\qquad T_e(0,r,z)=T_o \qquad (13.a)$

$$T_l(0,r,z)=T_o \qquad (13.b)$$

The mechanism for machining with femtosecond laser pulse is very different from the conventional laser machining. Where the pulse duration small and, there is no enough time for convection and radiation losses. In other words, no heat will release from the upper boundary of the target, see **Fig. 1.a.**

At $z=0$, $\qquad \left.\frac{\partial T_e(t,r,0)}{\partial z}\right|_{z=0}=0 \qquad (14.a)$

$$\left.K_l\frac{\partial T_l(t,r,0)}{\partial z}\right|_{z=0}=\rho L V_{sv} \qquad (14.b)$$

Select the origin point of the domain into, the center of the upper surface of the target, from symmetry of the cylindrical geometry. The boundary conditions obtained as follows:

At $r = 0$, $$\left.\frac{\partial T_e(t,0,z)}{\partial r}\right|_{r=0} = 0 \quad (15.a)$$

$$\left.\frac{\partial T_l(t,0,z)}{\partial r}\right|_{r=0} = 0 \quad (15.b)$$

The nature of the femtosecond laser ablation is different. Therefore, diffusion effect is very little in comparison with the conventional mechanisms. As a result, that the bottom surface of the material target considered insulated **Alan, and David, 1973.** These words also right for the distance far in the radial direction.

At $z = L_{ab}$, $$\left.\frac{\partial T_e(t,r,L_{ab})}{\partial z}\right|_{z=L} = 0 \quad (16.a)$$

$$\left.\frac{\partial T_l(t,r,L_{ab})}{\partial z}\right|_{z=L} = 0 \quad (16.b)$$

At $r = L_{ab}$, $$\left.\frac{\partial T_e(t,L_{ab},z)}{\partial r}\right|_{r=L} = 0 \quad (17.a)$$

$$\left.\frac{\partial T_l(t,L_{ab},z)}{\partial r}\right|_{r=L} = 0 \quad (17.b)$$

3. NUMERICAL SOLUTION

A numerical solution of Eq. (12) depends upon the explicit finite difference technique to calculate the electron and lattice temperature distribution of plume through r and z axes. The scripts T and F used for the electron and lattice temperatures respectively, then the indices i and j will be used for indicating the points along the r and z directions respectively, and the index n will be used for indicating the points over the time layers. We shall use the approximation of the first order of accuracy for time, and of the second order of accuracy for space. The distances between the points in the established grid are $\Delta r, \Delta z, and \Delta t$ .The grid is represented by **Fig. 1.c.** The finite difference form of Eq.(12) with explicit formulation, **Anderson, et al., 1984.** :

For electron subsystem:

$$T_{i,j}^{n+1} = T_{i,j}^{n}\left(1 - \frac{4K_e\Delta t}{C_e\Delta r^2} - \frac{\gamma\Delta t}{C_e}\right) + T_{i+1,j}^{n}\left(\frac{K_e\Delta t}{C_e\Delta r^2} + \frac{K_e\Delta t}{2C_e r_i\Delta r}\right) + \frac{K_e\Delta t}{C_e\Delta r^2}\left(T_{i,j+1}^{n} + T_{i,j-1}^{n}\right) + \frac{\Delta t\gamma}{C_e}F_{i,j}^{n} + \frac{\Delta t}{C_e}S_{ab} \quad (18.a)$$

For lattice subsystem

$$F_{i,j}^{n+1} = F_{i,j}^{n}\left(1 - \frac{4K_l\Delta t}{C_l\Delta r^2} - \frac{\gamma\Delta t}{C_l}\right) + F_{i+1,j}^{n}\left(\frac{K_l\Delta t}{C_l\Delta r^2} + \frac{K_l\Delta t}{2C_l r_i\Delta r}\right) + F_{i-1,j}^{n}\left(\frac{K_l\Delta t}{C_l\Delta r^2} - \frac{K_l\Delta t}{2C_l r_i\Delta r}\right) + F_{i,j+1}^{n}\left(\frac{K_l\Delta t}{C_l\Delta r^2} - \frac{V_{sv}\Delta t}{2\Delta z}\right) + F_{i,j-1}^{n}\left(\frac{K_l\Delta t}{C_l\Delta r^2} + \frac{V_{sv}\Delta t}{2\Delta z}\right) + \frac{\Delta t\gamma}{C_l}T_{i,j}^{n} \quad (18.b)$$

The Eq. (18) is so-called explicit formulation of Eq. (12). Then after applying the boundary conditions, the governing equation for every zone in the solution domain is:

1. At $r=0$ and $z=0$. $T^n_{i-1,j}=T^n_{i+1,j}$ and $F^n_{i-1,j}=F^n_{i+1,j}$ and $T^n_{i,j-1}=T^n_{i,j+1}$ and $F^n_{i,j-1}=F^n_{i,j+1}$ Eq. (18) can be re-written in the central difference form as:

$$T^{n+1}_{i,j}=T^n_{i,j}\left(1-\frac{4K_e\Delta t}{C_e\Delta r^2}-\frac{\gamma\Delta t}{C_e}\right)+T^n_{i+1,j}\left(\frac{2K_e\Delta t}{C_e\Delta r^2}\right)+\frac{2K_e\Delta t}{C_e\Delta r^2}\left(T^n_{i,j+1}\right)+\frac{\Delta t\gamma}{C_e}F^n_{i,j}+\frac{\Delta t}{C_e}S_{ab} \quad (19.a)$$

$$F^{n+1}_{i,j}=F^n_{i,j}\left(1-\frac{4K_l\Delta t}{C_l\Delta r^2}-\frac{\gamma\Delta t}{C_l}\right)+F^n_{i+1,j}\left(\frac{2K_l\Delta t}{C_l\Delta r^2}\right)+F^n_{i,j+1}\left(\frac{2K_l\Delta t}{C_l\Delta r^2}\right)+\frac{\Delta t\gamma}{C_l}T^n_{i,j} \quad (19.b)$$

2. At $0\langle r\langle L$ and $z=0$. $T^n_{i,j-1}=T^n_{i,j+1}$ and $F^n_{i,j-1}=F^n_{i,j+1}$ Eqns. (18) can be re-written in the central difference form as:

$$T^{n+1}_{i,j}=T^n_{i,j}\left(1-\frac{4K_e\Delta t}{C_e\Delta r^2}-\frac{\gamma\Delta t}{C_e}\right)+T^n_{i+1,j}\left(\frac{K_e\Delta t}{C_e\Delta r^2}+\frac{K_e\Delta t}{2C_e r_i\Delta r}\right)+T^n_{i-1,j}\left(\frac{K_e\Delta t}{C_e\Delta r^2}-\frac{K_e\Delta t}{2C_e r_i\Delta r}\right)+$$
$$+T^n_{i,j+1}\left(\frac{2K_e\Delta t}{C_e\Delta r^2}\right)+\frac{\Delta t\gamma}{C_e}F^n_{i,j}+\frac{\Delta t}{C_e}S_{ab} \quad (20.a)$$

$$F^{n+1}_{i,j}=F^n_{i,j}\left(1-\frac{4K_l\Delta t}{C_l\Delta r^2}-\frac{\gamma\Delta t}{C_l}\right)+F^n_{i+1,j}\left(\frac{K_l\Delta t}{C_l\Delta r^2}+\frac{K_l\Delta t}{2C_l r_i\Delta r}\right)+F^n_{i-1,j}\left(\frac{K_l\Delta t}{C_l\Delta r^2}-\frac{K_l\Delta t}{2C_l r_i\Delta r}\right)+$$
$$F^n_{i,j+1}\left(\frac{2K_l\Delta t}{C_l\Delta r^2}\right)+\frac{\Delta t\gamma}{C_l}T^n_{i,j} \quad (20.b)$$

3. At $r=0$ and $0\langle z\langle L$. $T^n_{i-1,j}=T^n_{i+1,j}$ and $F^n_{i-1,j}=F^n_{i+1,j}$ Eq. (18) can be re-written in the central difference form as:

$$T^{n+1}_{i,j}=T^n_{i,j}\left(1-\frac{4K_e\Delta t}{C_e\Delta r^2}-\frac{\gamma\Delta t}{C_e}\right)+T^n_{i+1,j}\left(\frac{2K_e\Delta t}{C_e\Delta r^2}\right)+\frac{K_e\Delta t}{C_e\Delta r^2}\left(T^n_{i,j+1}+T^n_{i,j-1}\right)+\frac{\Delta t\gamma}{C_e}F^n_{i,j}+$$
$$\frac{\Delta t}{C_e}S_{ab} \quad (21.a)$$

$$F^{n+1}_{i,j}=F^n_{i,j}\left(1-\frac{4K_l\Delta t}{C_l\Delta r^2}-\frac{\gamma\Delta t}{C_l}\right)+F^n_{i+1,j}\left(\frac{2K_l\Delta t}{C_l\Delta r^2}\right)+F^n_{i,j+1}\left(\frac{K_l\Delta t}{C_l\Delta r^2}-\frac{V_{sv}\Delta t}{2\Delta z}\right)+$$
$$F^n_{i,j-1}\left(\frac{K_l\Delta t}{C_l\Delta r^2}+\frac{V_{sv}\Delta t}{2\Delta z}\right)+\frac{\Delta t\gamma}{C_l}T^n_{i,j} \quad (21.b)$$

4. Apply Eqns. (18) when
$0<r<L\ and\ 0<z<L.$

$\left(1-\frac{4K_e\Delta t}{C_e\Delta r^2}-\frac{\gamma\Delta t}{C_e}\right)$ Is the convergence term as described by references, **Alan, and David, 1973.** , and **Anderson, et al., 1984.** Where the convergence criteria mentioned that the value of the convergence term must be greater than or equal zero, to avoid solution fluctuation:

The electron and lattice temperature distribution through r-z plane, where $r=2$ to $L-1$ and $z=2$ to $L-1$ is represented as shown in **Fig. 1.b**. A special

consideration is carried out for the exterior nods, with aid of factious points to mesh. The computer program was built in Visual FORTRAN language and run on pentium4 PC, using operating system Microsoft XP. Run time of about several minutes was needed to achieve the required convergence.

4. REULTES AND DISCUSSION

Figs. 2 to 5 explain the electron and lattice subsystem reduced temperature temporal distribution through the time with respect to laser pulse duration. Form these figures can be conclude that the temperature of the electron subsystem raised rapidly and approached to peak value at the end of laser pulse duration because of that the electron heat capacity is less than the lattice heat capacity. Electrons absorb the laser energy i.e., where the free electrons absorb the incident energy of the laser pulse due to invers-Bremsstrahlnug **Grojo, et al., 2003** and **Zeng,** and **Xianzhong, 2004.** In addition the electron heat capacity is low in comparison with the lattice-subsystem heat capacity, **Mannion, et al., 2001.** At the end of the pulse duration the temperature of the electron subsystem will decrease rapidly sometimes suddenly due to the electron-phonon (lattice) coupling and energy transfer to the lattice subsystem, as shown in **Figs. 4 and 5**.

In accordance with the different in the heat capacities of electron and lattice subsystems, the lattice temperature subsystem not much increase in compared with the electron subsystem. Briefly the behavior of electron and lattice can be expressed as the electron temperature will be increased rapidly until the end of laser pulse, then decreased rapidly. Moreover for the lattice subsystem, the temperature profile increased slowly form the beginning of laser pulse and remain increased after the end of pulse duration (for several pulse duration times), due to large heat capacity for the lattice subsystem, **Cheng, and Xu, 2005.**

The electron temperature reaches peak value at the end of laser pulse. It can also be seen that till this time the lattice remains virtually cold. Subsequently, the initial laser energy is totally absorbed by the electrons within the optical penetration depth. These energetic electrons move at very high speeds on the order of ~ 106 m/s. Subsequently, the electrons reach thermal equilibrium and diffuse deeper into the material at reduced speeds. It is only at a much longer time scale that energy transfer to the lattice occurs. Thereafter, both the electrons and the lattice reach the same temperature, and at long time scales > 40 ps they behave as a single system. Beyond this time, heat transfer occurs by conduction at much lower speeds, **Chimmalgi, et al., 2005.** Therefore, it can be stated that the calculations consistence with the published results.

In comparison between **Figs. 2, 3** for nickel and **Figs. 4, 5** for copper, it can be noticed that the reduced temperature profile for electron subsystem of copper metal is suddenly decreased after pulse duration due to electron-phonon relaxation coupling.

Figs. 6 and **7** show the electron and lattice subsystems reduced temperature profiles (T/T_C) versus the reduced radius (r/R) at time (1 tp), "the end of laser pulse". These figures indicate that the electron and lattice temperatures reach the peak value at the center of the laser crater because of Gaussian distribution of the laser beam. In addition, the value of the electron temperature is much higher than the lattice temperature for the same reasons as in **Figs. 2** to **5**.

Figs. 8 and **9** explain the electron and lattice subsystems reduced temperature (T/T_C) versus the reduced depth (z/R) at the end of pulse. These figures show that in spite of that the free electrons in the surface layer of target metal absorbs the laser beam energy, that the free electrons in the depth of metal target are also absorbs the

energy of the transmitted part of the irradiated beam. Finally, the energy of the electron subsystem is transferred to lattice subsystem; after several times of pulse duration. In addition, that the reduced temperature profile will be decreased gradually with depth. Finally the temperature profile for the electron and lattice subsystems will be approached the same value at the distance far from the surface of the metal target.

At different pulse duration times, **Figs. 10** and **12** indicate the spatial temperature distribution for electron subsystem. The temperature curve for every figure show that the temperature increased with time and reached the maximum value at time equals 1 tp, and then the temperature will be decreased rapidly and approached initial value after several tp. It can be noticed that the temperature profile in the radial and depth direction approximately the same.

Figs. 11 and **13** show the distribution of reduced lattice temperature spatially for different pulse duration times in the radial and depth directions. From these figures, it can be noticed that the reduced temperature levels is less than the reduced temperature values in **Figs. 10** and **12** respectively, where the heat capacity of lattice subsystem is greater than that of electron subsystem, **Qiu, & Tien, 1993.** The reduced lattice temperature approaches the peak value at time equals 5 tp. In comparison with **Figs. 10** and **12,** it can be concluded that the lattice subsystem gain the heat slowly, but the free electrons absorb heat rapidly and radiant it at high rate.

Figs. 14 and **15** plot the isothermal contour map for reduced electron and lattice temperature in the rz-plane for copper. These two figures indicate the big difference in the temperature levels between the free electron and lattice subsystem, for the same conditions.

5. CONCLUSION

The time evolution for temperature of electron subsystem is faster than the temperature of lattice subsystem. Where, the heat capacity of the lattice was higher than the heat capacity of the free electrons. The metal target treated as two subsystems, in the ultra-short pulsed laser irradiation. The plasma plume existence in the ultra-short pulsed laser where, the temperatures of the electron and lattice subsystems exceed the critical temperature.

The weaker non-equilibrium between the electron and lattice (phonon) during the laser pulse reduce the ablation rate, and vies versa especially for Nickel. Nickel has a shorter lattice response time than for the copper. As explained in **Figs. 2** to **5**.

As a rule, the models employed in the theory of laser ablation are reliant on complex nonlinear systems of partial differential equations whose solution calls for the use of numerical methods.

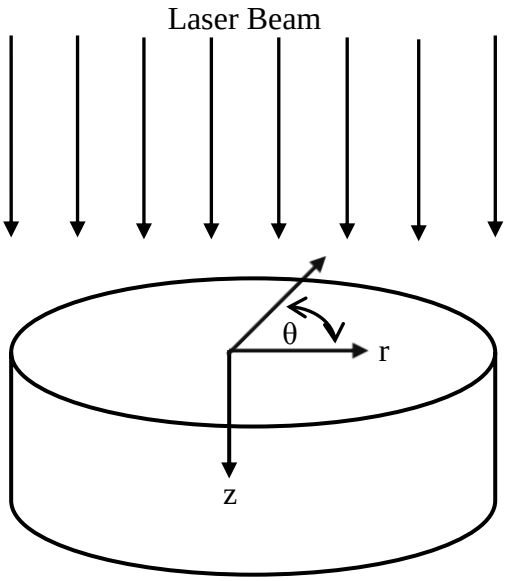

(a) Schematic of the computational domain

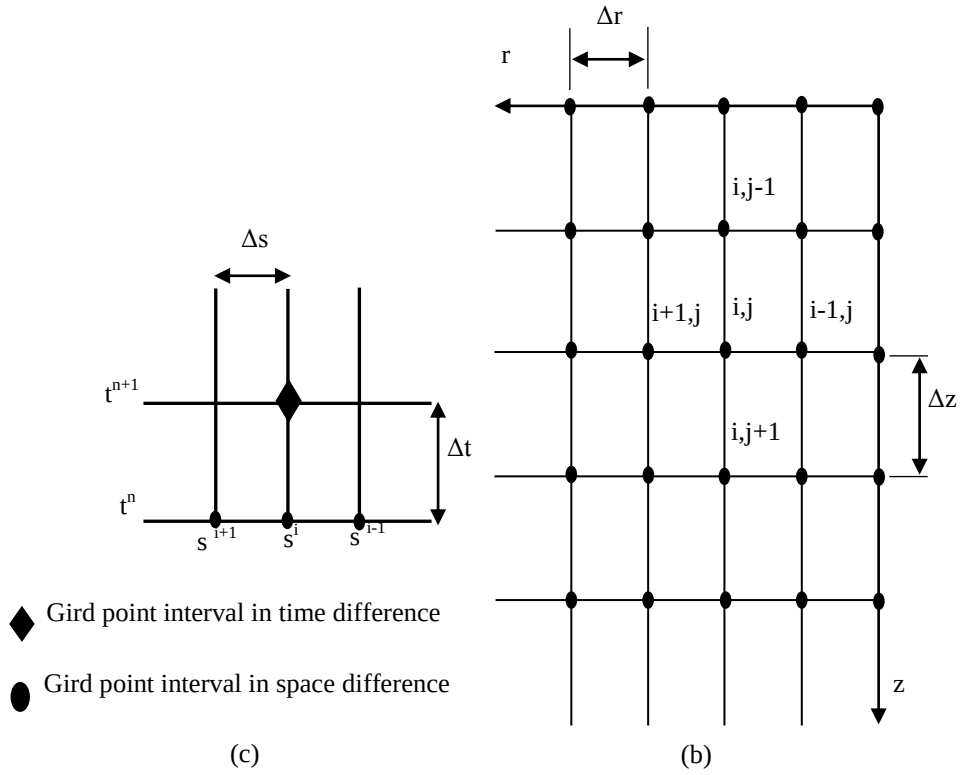

Figure 1. Type of fixed boundary conditions for electron and lattice temperature distributions.

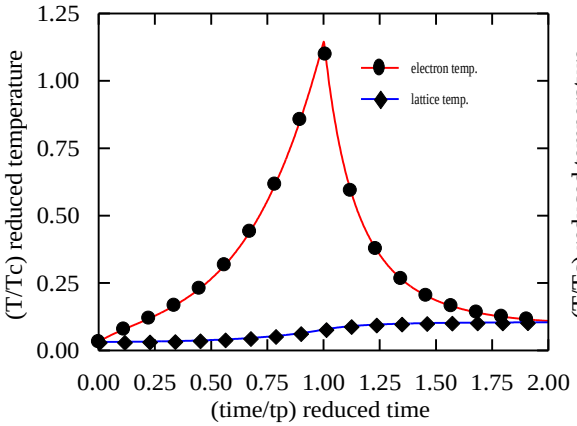

Figure 2. Reduced Lattice & Electron Temp. vs. the Pulse Duration Time for tp=0.5E-12 S, J_f=0.27 J/cm^2 Metal:Nickel

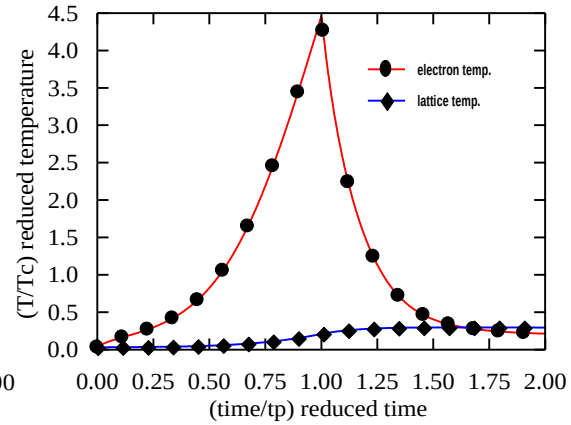

Figure 3. Reduced Lattice & Electron Temp. vs. the Pulse Duration Time for tp=0.5E-12 S, J_f=1.0 J/cm^2 Metal:Nickel

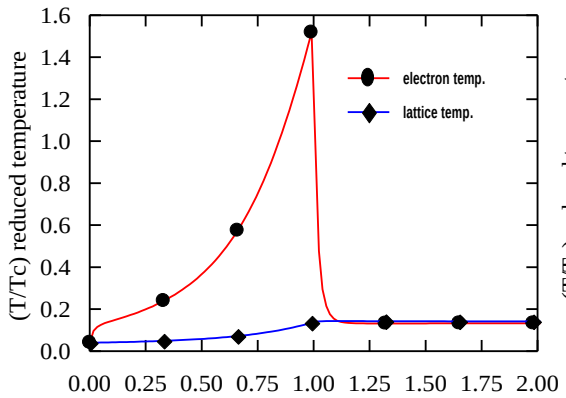

Figure 4. Reduced Lattice & Electron Temp. vs. the Pulse Duration Time for tp=0.5E-12 S, J_f=0.3529 J/cm^2 Metal:Copper

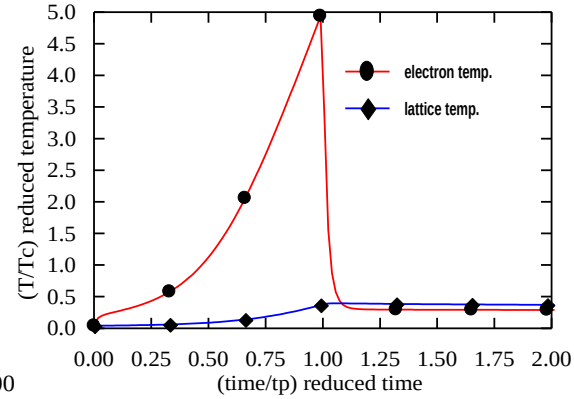

Figure 5. Reduced Lattice & Electron Temp. vs. the Pulse Duration Time for tp=0.5E-12 S, J_f=1.0 J/cm^2 Metal:Copper

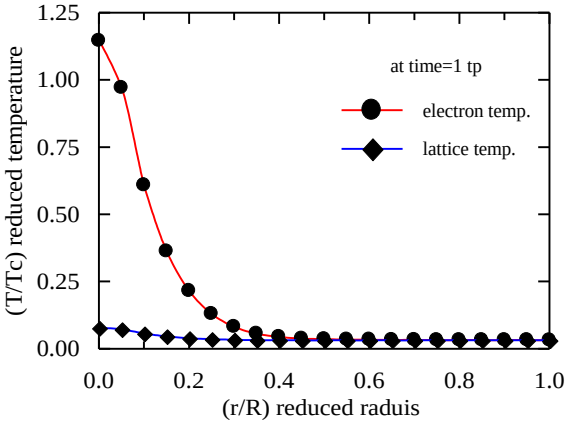

Figure 6. Reduced Lattice & Electron Temp. vs. Radial Dist for tp=0.5E-12 S, J_f=0.27 J/cm^2 Metal:Nickel

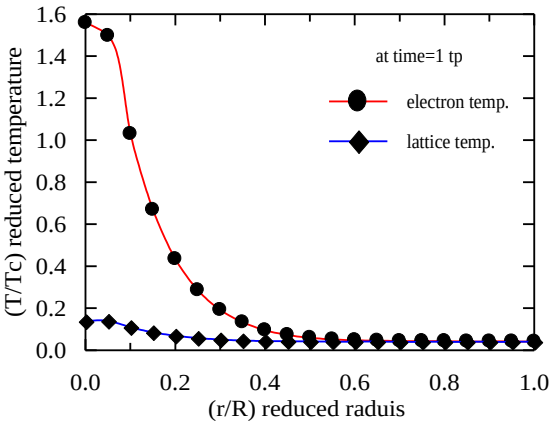

Figure 7. Reduced Lattice & Electron Temp. vs. Radial Dist. for tp=0.5E-12 S, J_f=0.3529 J/cm^2 Metal:Copper

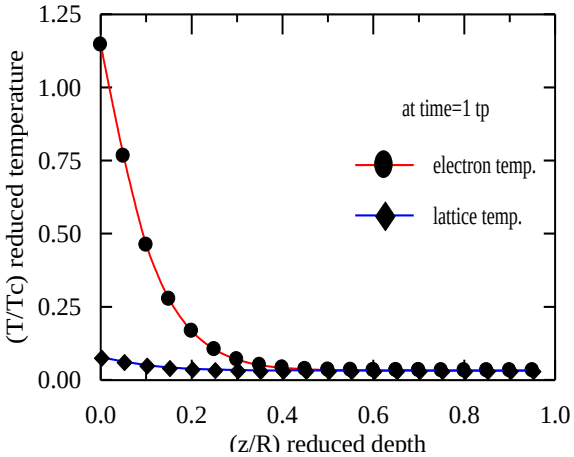

Figure 8. Reduced Lattice & Electron Temp. vs. Reduced Depth Dist. for tp=0.5E-12 S, J_f=0.27 J/cm^2 Metal:Nickel

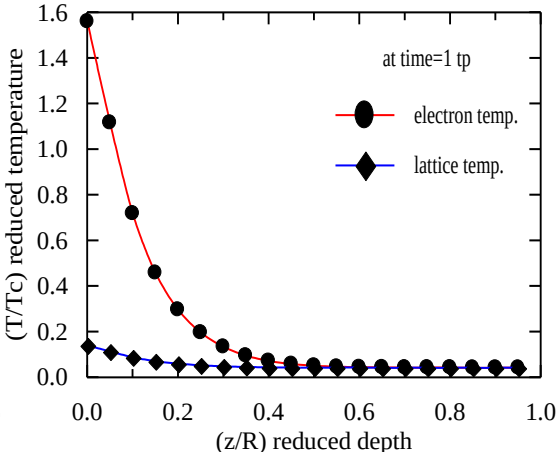

Figure 9. Reduced Lattice & Electron Temp. vs. Reduced Depth Dist. for tp=0.5E-12 S, J_f=0.3529 J/cm^2 Metal:Copper

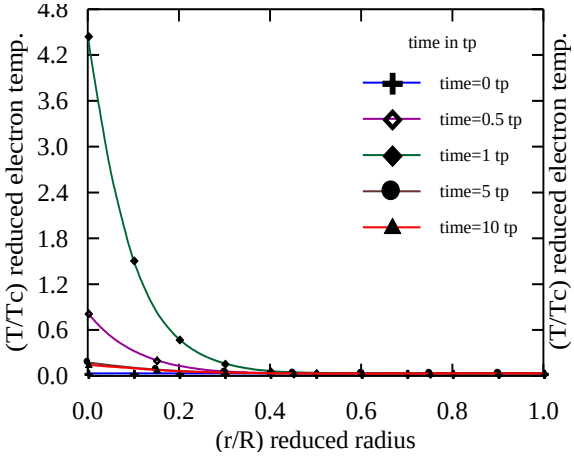

Figure 10. Reduced Electron Temp. for Different Pulse Duration Times vs. Reduced Raduis for tp=0.5E-12 S, J_f=0.3529 J/cm^2 Metal:Nickel

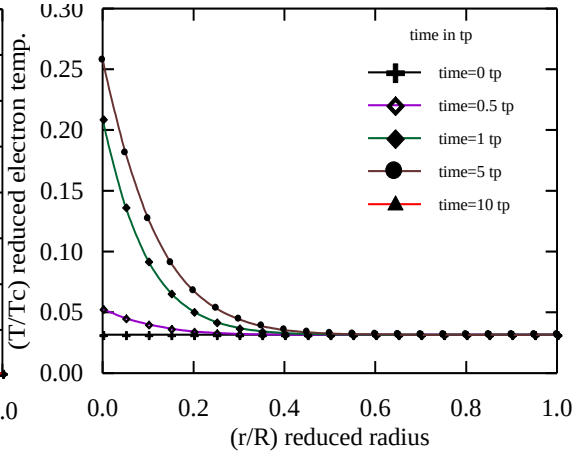

Figure 11. Reduced Lattice Temp. for Different Pulse Duration Times vs. Reduced Raduis for tp=0.5E-12 S, J_f=1.0 J/cm^2 Metal:Nickel

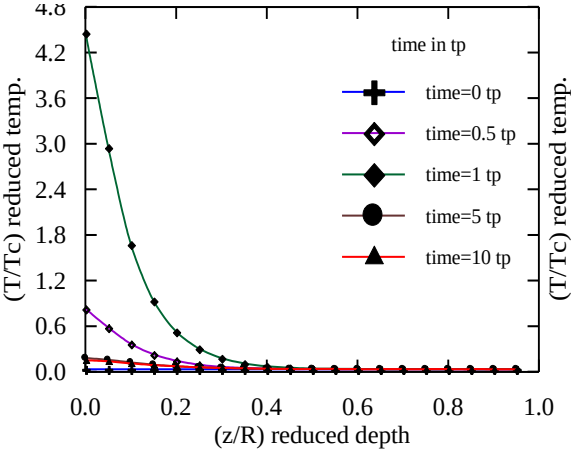

Figure 12. Reduced Electron Temp. for Different Pulse Duration Times vs. Reduced Depth for tp=0.5E-12 S, J_f=1.0 J/cm^2 Metal:Nickel

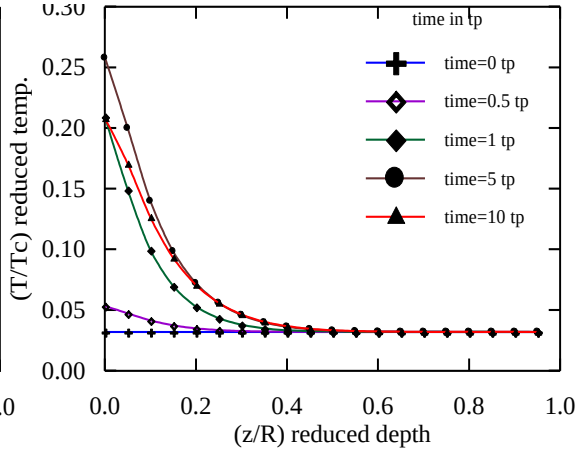

Figure 13. Reduced Lattice Temp. for Different Pulse Duration Times vs. Reduced Depth for tp=0.5E-12 S, J_f=1.0 J/cm^2 Metal:Nickel

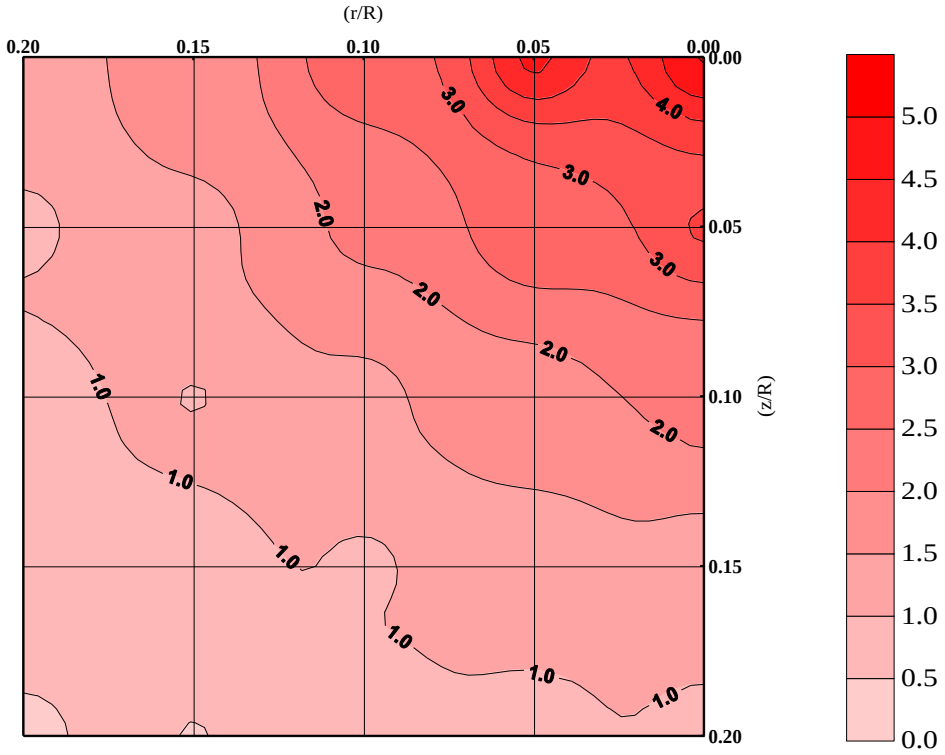

Figure(14): Isothermal contour map of reduced electron temp.vs. the normlized r-z palne for tp=0.5E-12 sec Jf=1.0 J/cm^2 metal:Copper

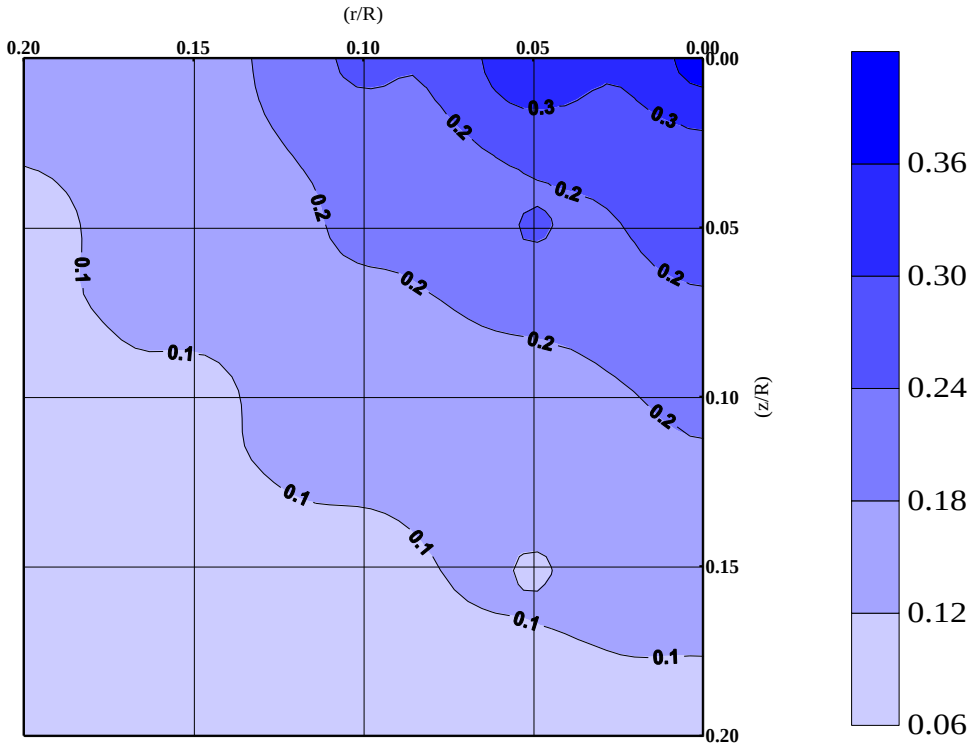

Figure(15): Isothermal contour map of reduced lattice temp.vs. the normlized r-z palne for tp=0.5E-12 sec Jf=1.0 J/cm^2 metal:Copper

NOMENCLATURES

Sample	*Description*	*Unite*
C_e	specific heat of electron subsystem	$J/m^3.K$
C_l	specific heat of lattice subsystem	$J/m^3.K$
D_e	electron diffusion coefficient	m^2/S
E	energy transferred	J
E_f	fermi energy	J
e	subscript denotes the electron subsystem	--
l	subscript denotes the lattice subsystem	--
I	laser power intensity	W/cm^2
i, j	The indexes increase along the r, z	--
J_f	incident laser fluence	W/m^2
K_e	electron thermal conductivity coefficient	$W/m.K$
K_l	lattice thermal conductivity coefficient	$W/m.K$
k_B	Boltzmann constant	
L_{sv}	enthalpy of sublimation per atom	J/kg
m	electron mass	kg
n_e	electron density	m^{-3}
n	index increases along the time	--
R	material reflectivity	--
r	radial distance	m
r_{ab}	radius of ablation crater	m
S_{ab}	source in the governing equation	S
t	time	S
t_p	laser pulse duration time	S
T_e	electron temperature	K
$T_{i,j}^n$	electron temperature in numerical form	K
T_l	lattice temperature	K
$F_{i,j}^n$	lattice temperature in numerical form	K
T_F	Fermi temperature	K
T_o	ambient temperature	K
T_b	boiling temperature	K
T_c	critical temperature	K
V_{sv}	solid-vapor interface velocity	m/S
α	material dependent parameter	--
ρ	material density	Kg/m^3
τ	electron relaxation time which is determined by electron-electron and electron-phonon collisions.	S
γ	coefficient of electron-lattice relaxation rate	$W/m^3.K$
v_F	electron velocity	m/S
δ_{ab}	absorption ablation depth	m

REFERENCES

Al-moosawy, Adil, A., 2002, *Modeling of Thermal History of Solid Material Processed by Laser* , Ph.D. Thesis, University of Technology, Mech. Dept.,.

Alan Adams, J., and David, F., Rogers., 1973, *Computer-Aided Heat Transfer Analysis*, McGraw-Hill,.

Anderson, D. A., Tannehill, J. C., and Pletcher, R. H., 1984, *Computational Fluid Mechanics and Heat Transfer,* McGraw-Hill,.

Bulgakova, M., Nadezhda, M., Igor, Burakov, Meshcherykov, Yuri, P., Stoian, Razvan, Rosenfeld, Arkadi, and Hertel, Ingolf, V., 2007,*Theoretical Models and Qualitative Interpretations of Fs Laser Material Processing*, JLMN-Journal of Laser Micro/Nanoengineering Vol. 2, No. 1,.

Chimmalgi, A., Grigoropoulos, C., P., and Komvopoulos, K., 2005, *Surface Nanostructuring by Nano-femtosecond Laser-assisted Scanning Force Microscopy*, Journal of Applied Physics, 97, 104319.

Cheng, Changrui, and Xu, Xianfan, 2005, *Mechanisms of Decomposition of Metal during Femtosecond Laser Ablation*, Physical Review B,72,165415,.

Grojo, D., Hermann, J., Bruneau, S., and Itina, T., 2003, Analyses of Femtosecond Laser Ablation of Ti, Zr and Hf, LP3-FRE 2165 CNRS,Faculté des Sciences de Luminy,Case 917,13288 Marseille Cedex 9,France.

Hermann, J., Benfarah, M., Coustillier, G., Bruneau, S., Axente, E., Guillemoles, J.,-F., Sentis, M., Alloncle, P., Itina, T., 2005, *Selective Ablation of Thin Films with Short and Ultrashort Laser Pulses*, Applied Surface Science.

Harrach, R. J., Dec. 1977, *Analyatic Solutions for Laser Heating and Burn-through of Opaque Slabs,* J. Appl. Phys., Vol. 48, pp. 2370-2375.

J.P. Colombier, P. Combis, F. Bonneau, R. Le Harzic, and E. Audouard., 2006, *Hydrodynamic Simulations of Metal Ablation by Femtosecond Laser Irradiation*, Dept. de Physique Th´eorique et Appliqu´ee ,France.

Korte, F. Adams S., Egbert, A. Fallnich, C. Ostendorf, A., 17July, 2000, *Sub-diffraction Limited Structuring of Solid Targets with Femtosecond Laser Pulses,* Institute of Applied Physics, Friedrich-Schiller-University Jena, Vol.7, No.2/Optics Express,Jena,Germany.

Leitz, Karl-Heinz, Redlingshöfer, Benjamin, Reg, Yvonne, Otto, Andreas, Schmidt, Michael, 2011, *Metal Ablation with Short and Ultrashort Laser Pulses*, Physics Procedia 12, 230–238.

Mannion, P. T., Favre, S., Mullan, C., Ivanov, D. S., O'Connor, G. M., Glynn, T. J., Doggett, B., and, Lunney, J. G., 2002, *Langmuir Probe Investigation of Plasma*

Expansion in Femto and Picosecond Laser Ablation of Selected Metals ,National Centre for Laser Applications, NUI Galway, Ireland.

Mannion, Paul, Magee, Jonathan, Coyne, Edward, and M., O'Connor, Gerard, 2001, *Ablation Thresholds in Ultrafast Laser Micro-machining of Common Metals in Air*, National Centre for Laser Applications, National University of Ireland, Galway, Ireland, Proc. of SPIE Vol. 4876.

N.W. Ashcroft and N.D. Mermin, *Solid State Physics* ,Saunders College Publishing, New York,1976.

Qiu, T. Q., and Tien, C. L., 1993, *Heat Transfer Mechanisms During Short-pulse Laser Heating of Metals* ASME J. Heat Transfer, 115, pp. 835–841.

Schäfer, C.; Urbassek, H.M.; Zhigilei, L.V., 2002,*Metal Ablation by Picosecond Laser Pulses: A hybrid simulation*. Phys. Rev. B, in press.

S.I. Anisimov, B.S. Luk'yanchuk, A. Luches, 1996, *An Analytical Model for Three-dimensional Laser Plume Expansion into Vacuum in Hydrodynamic Regime*, Appl. Surface Science 96-98, pp 24-32.

S.I. Anisimov and B. Rethfeld, Izv. Ross. Akad. Nauk, Ser. Fiz. 61, 1642, 1997.

Xianfan Xu , 2004, *Molecular Dynamics Study of Phase Change Mechanisms During Femtosecond Laser Ablation*, Journal of Heat Transfer (ASME).

Zhigilei, Leonid, V., and Dongare, Avinash, M., 2002, *Multi-scale Modeling of Laser Ablation: Applications to Nanotechnology*, CMES, vol.3, no.5, pp.539-555,

Zeng, Xianzhong, 2004,*Laser Ablation of Electronic Materials Including the Effects of Energy Coupling and Plasma Interactions*, Ph.D. Thesis, University of California, Berkeley.